



PERGAMON

Continental Shelf Research 21 (2001) 545–561

CONTINENTAL SHELF
RESEARCH

www.elsevier.com/locate/csr

Tide observations in the Korea-Tsushima Strait

W.J. Teague*, H.T. Perkins, G.A. Jacobs, J.W. Book

Naval Research Laboratory, Stennis Space Center, MS 39529, USA

Received 10 April 2000; accepted 12 September 2000

Abstract

Tides are analyzed in the Korea-Tsushima Strait using measurements from 11 moorings, each containing an acoustic Doppler current profiler (ADCP) and a pressure gauge. These instruments were bottom moored at depths ranging from 59 to 142 m from May 1999 until October 1999 along two lines across the Strait, northeast and southwest of Tsushima Island. Tide amplitudes range over 3 m along the southern line but only range about 0.7 m along the northern line. Maximum total current velocities exceed 100 cm/s in the surface layers and typically exceed 50 cm/s at mid-depths along both lines. These data are analyzed for eight tidal constituents, which are found to account for about 88% of the sea surface height variability along the southern line and 70% along the northern line. M₂, S₂, K₁, and O₁ are the dominant constituents. Their amplitudes are generally 10–20% smaller than amplitudes from tide charts. M₂ tidal velocities range from 17 to 25 cm/s along the line northeast of Tsushima Island, and are largest at the mooring on the western side of the Strait, nearest to Korea. Southeast of Tsushima Island, either M₂ or K₁ dominates the tidal contribution to the current, with tidal velocities ranging between 13 and 23 cm/s. Tidal velocities are fairly depth independent at mid-depths but exhibit varying degrees of depth dependence in the near-surface and near-bottom layers. While tidal currents are responsible for about 25% of the eddy kinetic energy in the near surface layer, they account for more than 50% of the eddy kinetic energy at mid-depths and about 70% near the bottom. © 2001 Elsevier Science Ltd. All rights reserved.

Keywords: Tides; Tidal currents; Acoustic current meters; Bottom pressure; Coastal oceanography; Korea-Tsushima Strait

1. Introduction

Long-term measurements of currents and tidal elevations in the interior of the Korea-Tsushima Strait (hereafter referred to as the Strait) are rare because of the intense level of fishing and trawling (Kawatate et al., 1988). However, there have been many short-term measurements that

*Corresponding author. Tel.: +1-228-688-4734; fax: +1-228-688-5997.

E-mail address: teague@nrlssc.navy.mil (W.J. Teague).

have estimated the general strength of the currents and tides (Mizuno et al., 1989; Egawa et al., 1993; Isobe et al., 1994; Katoh et al., 1996). These studies find the currents and tides to be very complex and emphasize the need for long-term measurements in the Strait.

The Strait is a narrow and shallow connecting channel between the broad, shallow Yellow and East China Seas (depths of 50–1000 m) and the deeper East/Japan Sea (hereafter referred to as the Japan Sea; depths exceeding 2000 m). In general, the dimensions of the Strait are about 180 km in width, 330 km in length, and a mean water depth of about 100 m. Through this strait the major influx of seawater enters the Japan Sea and thus determines the transfer of heat, salt, fish larvae, etc. into the Japan Sea.

Extensive studies by Ogura (1933) provide the present conception of the tidal current activity in the Strait. He describes the tides in the Strait as a complex mixture of longitudinal oscillations along the axis of the Strait and transverse oscillations across the Strait. He attributes the latter to the earth's rotation and the former to the progression of the tide wave back and forth between the East China Sea and the Japan Sea. Ogura (1933) shows that this combination of motions results in an amphidromic point for the semidiurnal tide at about 35.5°N, 130°E, and for the diurnal tide at about 35.2°N, 130.5°E. The semidiurnal tidal wave rotates counterclockwise around the amphidromic point. More recently, Odamaki (1989) shifted both of these amphidromic points somewhat towards Korea based on analysis of simultaneous tides and tidal currents. The range of the tide increases southward through the Strait from the Japan Sea into the East China Sea by about a factor of 10. Tidal currents with speeds approaching 50 cm/s embedded in currents with speeds of nearly 100 cm/s have been reported in the Strait by Isobe et al. (1994).

The recent development of trawl resistant instrument mounts for mooring instruments on the bottom makes long-term measurements possible in the Strait. This technique was recently used in the Yellow Sea to deploy acoustic Doppler current profilers (ADCPs) and pressure gauges (Teague et al., 1998; Teague and Jacobs, 2000). This study analyzes data from 11 similar moorings in the Strait that are located on lines nearly spanning the Strait on the northern and southern sides of Tsushima Island (Fig. 1). One purpose of these measurements is to delineate the structure of the currents and tides and thus gain a better understanding of the dynamics in the Strait. Using these measurements, Jacobs et al. (2000) estimate transports of 2.4 and 2.8 Sverdrups (Sv) with an error of about 0.5 Sv through the northern and southern lines, respectively. Perkins et al. (2000a) described the structure of the low-frequency current flows. Non-tidal flows exceed 30 cm/s in the middle of the Strait. The two sections show markedly different flow regimes. At the southern entrance, the cross-sectional flow varies smoothly across the channel, showing a broad maximum at mid-channel. The northern section, is marked by strong spatial variability, but in the mean consists of two streams, one on each side of the strait. Between the two is a regime of highly variable flow with a weak mean, presumably the wake from Tsushima Island. Vertically averaged mean currents with standard deviation ellipses are shown in Fig. 2. The center of the standard deviation ellipse is at the tip of the arrowhead, and reflects the area that is within one-standard deviation of the mean. Hence, the most probable current vector tip lies within the ellipse. Largest mean flow, about 30 cm/s, is found near the middle of the Strait, southwest of Tsushima Island. Mean current flows of nearly 20 cm/s are observed near both ends of the northern section. Tides are expected to significantly contribute to the total current flow in these regions.

Here, the tides are examined through analyses of both current and pressure measurements. These unique measurements allow determinations of the cross strait and vertical tidal structures.

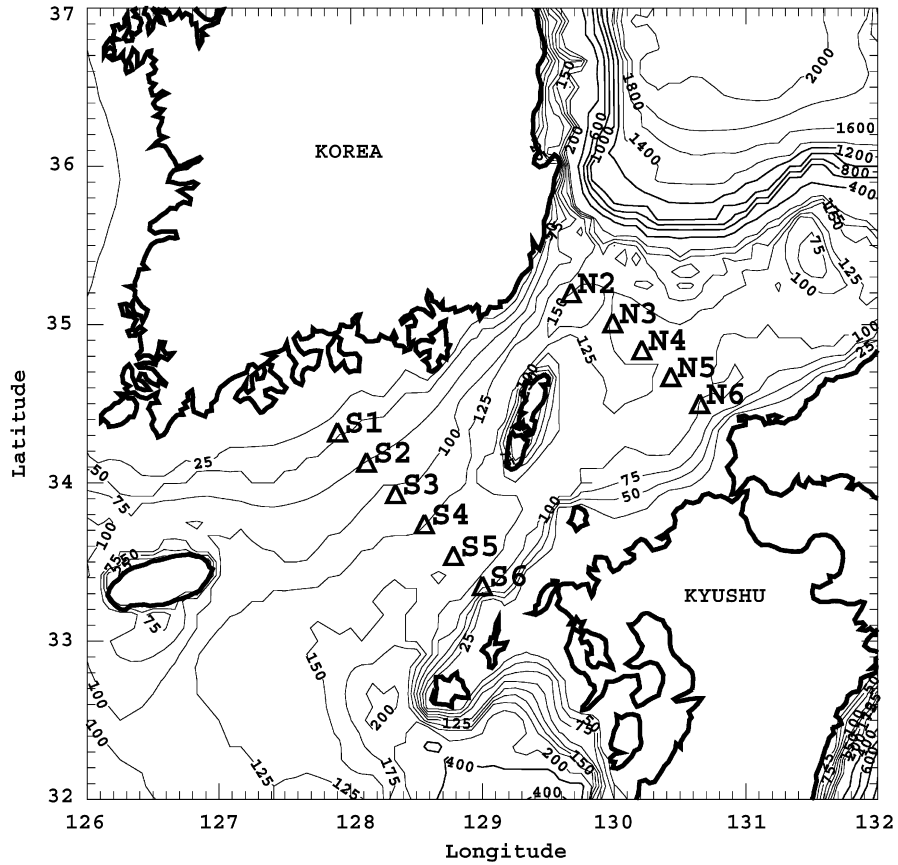


Fig. 1. ADCP and pressure gauge mooring locations, and bathymetry. Depths are in meters.

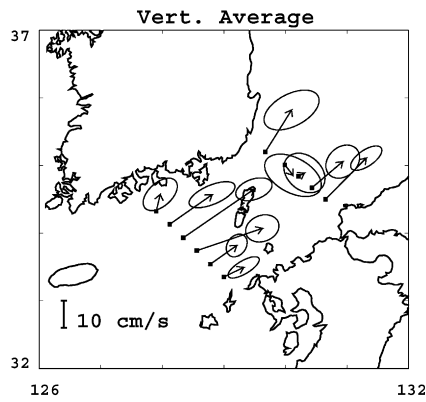


Fig. 2. Vertically averaged mean current vectors and standard deviation ellipses after tide removal.

Both the pressure and current measurements are analyzed for the eight dominant tidal constituents. Some significant differences in tide amplitudes and phases with tide chart values are found. The relative contribution of the tidal currents to the total currents are calculated. Current profiles measured by bottom moored ADCPs over long time periods are ideal for answering questions pertaining to the currents and tides which have never been adequately addressed due to the difficulty in making such measurements.

2. Instrumentation

Eleven moorings were deployed along two lines, northeast and southwest of Tsushima Island, in the Strait during May 1999 (Fig. 1). The line southwest of Tsushima is referred to as the south line (S1–S6) and the line northeast of Tsushima as the north line (N2–N6). Each deployed package consisted of an acoustic Doppler current profiler (ADCP) and a wave/tide gauge housed in a trawl-resistant bottom mount (TRBM). Nine of the deployments were based on a new type of TRBM known as Barnys after their barnacle-like shape (Perkins et al., 2000b). The Barnys were developed by SACLANT Center in Italy in collaboration with the Naval Research Laboratory (NRL). The remaining TRBMs, at sites N2, N3, and S5, were of a different design developed at the Naval Oceanographic Office (Teague et al., 1998). In general, both types of mounts are shallow dome-shaped enclosures that rest upon the bottom. The exposed side of the dome is relatively smooth in order to minimize snagging by fishing nets and lines.

The Barny mounts were equipped with RD Instruments Workhorse ADCPs operating at 300 KHz. The TRBMs from the Naval Oceanographic Office were equipped with RD Instruments Narrowband ADCPs operating at 150 KHz. All packages contained Sea-Bird Electronics Model 26 wave/tide gauges and EdgeTech Model 8202 acoustic releases for location and recovery. The instruments, protected within the mount, rest about 0.5 m above the ocean bottom. The ADCPs were set up to provide current profiles with an accuracy of 1 cm/s over nearly the full water column. Depth resolution is 2 m at S1, S2, and N2 and 4 m for the other ADCPs. Profiles of u (east–west) and v (north–south) components of velocity were recorded at 30 min intervals except at 15 min intervals at S5, N2, and N3. Pressure was recorded every 15 min. Since the pressure of 1 dbar corresponds approximately to the sea pressure exerted by a water column of 1 m, the pressure measurements will be referred to in terms of meters of sea water. Thus the pressure gauge data are converted into observations of height variability. The accuracy of each pressure gauge is about 3 cm. Since only mean atmospheric pressure is removed from the pressure data during processing, fluctuations in atmospheric pressure during the passage of storms may result in errors of 5–10 cm in height. Scraps of nets as well as evidence of trawl scrapings were found on the moorings at instrument retrieval. There was no evidence of these fishing activities in the data records. One mooring was not recovered. It was located northwest of N2 on the western end of the north line (site N1, not shown). The failure is attributed to the instrument sinking into the mud and is not due to an electronics or mechanical problem. Geographical positions, depths, and times for each of the moorings are summarized in Table 1.

Table 1
ADCP summary

Mooring	Lat	Lon	Start day	End day	Top bin	Bottom bin	Bin size	Water depth
S1	34.32	127.90	130	289	5	53	2	59
S2	34.13	128.12	129	289	7	83	2	89
S3	33.93	128.34	129	288	11	103	4	113
S4	33.74	128.56	128	287	9	97	4	107
S5	33.54	128.78	128	287	19	143	4	152
S6	33.35	129.00	128	286	9	105	4	115
N2	35.20	129.67	125	282	25	137	2	142
N3	35.01	129.99	126	283	13	125	4	132
N4	34.84	130.21	126	283	13	117	4	127
N5	34.67	130.43	127	284	16	120	4	130
N6	34.50	130.65	127	284	12	108	4	118

3. Tidal height analysis

Total tide amplitudes range over 3 m along the southern line and about 0.7 m along the northern line. Tides are known to decrease to less than 0.1 m in the central part of the East/Japan Sea (Kang et al., 1991). The pressure gauge (PG) data are analyzed with a tidal package (Foreman and Henry, 1979) which uses a least-squares analysis method incorporating nodal modulation, astronomical argument correction, and inference calculations for tidal amplitudes and phases. There is a maximum of 146 possible tidal constituents that can be included in the tidal analysis, 45 of these are astronomical in origin (main constituents) while the remaining 101 are shallow water constituents (Godin, 1972) which arise from distortion of the main tidal constituents in shallow water. Shallow water has the effect of retarding the speed of the trough of a wave more than the crest, since the speed of propagation of a shallow water wave is proportional to the square root of the water depth. After preliminary analysis, constituents with amplitudes of about a centimeter or less were removed from the analysis and the data were reanalyzed for the eight largest constituents (O1, P1, K1, MU2, N2, M2, S2, and K2). Amplitudes and Greenwich phases for these eight constituents are given in Table 2.

Tidal height amplitudes are larger on the southern line than on the northern line by a factor of three to four. The semi-diurnal M2 constituent is the dominant constituent followed by the S2 constituent along both lines. Next, largest amplitudes on the south line are observed at K1, and followed by either O1 or N2 constituents, which have comparable amplitudes. Amplitudes of the other constituents on the north line are less than 10 cm. The amplitudes of the M2 and S2 constituents decrease from west to east along the southern line (85–72 cm for M2 and 38–33 cm for S2). However, the corresponding amplitudes increase from west to east along the northern line (17–23 cm for M2 and 8–12 cm for S2). Shallow water tides such as M4 are small (less than a 1 cm).

The predicted tidal height, ζ_p , is formed by combining the eight main constituents. In order to estimate the contributions of the tides to the total variability, tidal residuals and normalized

residuals are calculated. Residual tide RMS, σ_r , is given by

$$\sigma_r = \sqrt{\frac{1}{T} \int_0^T (\zeta_p(t) - \zeta_o(t))^2 dt} \quad (1)$$

for a time series of length T , where ζ_o is the observed surface height after removal of the mean. The normalized residual is defined as σ_r/σ_o , where σ_o is the standard deviation of ζ_o . Tidal height residuals and normalized residuals are given in Table 3. Residual tide RMS values are smaller

Table 2

(a) Tide summary, south line — amplitude (cm)/greenwich phase

Tide	Period (h)	PG S1	PG S2	PG S3	PG S4	PG S5	PG S6
O1	25.82	14.6/32.8	13.5/42.2	13.4/51.8	13.8/59.5	14.8/66.9	16.3/73.0
P1	24.07	6.3/48.6	5.9/55.7	5.7/63.2	5.7/70.8	5.9/77.9	6.3/84.3
K1	23.93	19.8/56.3	18.3/63.8	17.7/71.6	17.8/78.4	18.6/85.6	20.0/91.8
MU2	12.87	3.8/347.0	3.6/348.8	3.4/349.2	3.4/351.9	3.4/353.3	3.4/355.0
N2	12.66	17.0/349.0	15.8/348.3	14.9/347.8	14.4/347.1	14.2/346.5	14.1/346.3
M2	12.42	85.0/357.6	79.0/356.5	75.0/355.7	72.9/354.6	72.0/353.8	72.0/353.3
S2	12.00	38.3/21.4	35.9/20.2	34.2/19.4	33.3/18.5	33.0/17.7	32.9/17.2
K2	11.97	10.3/13.8	9.5/12.1	9.1/10.9	8.8/9.9	8.7/9.2	8.7/7.6

(b) Tide summary, north line — amplitude (cm)/Greenwich phase

Tide	Period (h)	PG N2	PG N3	PG N4	PG N5	PG N6
O1	25.82	2.2/169.7	3.6/149.1	5.1/142.2	6.9/142.4	9.1/143.4
P1	24.07	0.2/152.2	0.9/140.1	1.4/144.6	2.0/147.6	2.6/151.1
K1	23.93	1.0/204.5	2.6/163.5	4.4/157.7	6.4/160.6	8.6/164.7
MU2	12.87	0.8/349.3	0.9/3.5	1.0/13.7	1.1/18.1	1.2/26.1
N2	12.66	3.1/330.0	3.3/346.7	3.6/357.4	4.0/6.4	4.4/14.7
M2	12.42	17.0/339.3	18.2/352.9	19.7/2.3	21.3/11.0	23.1/18.8
S2	12.00	8.8/8.4	9.5/18.9	10.3/26.6	11.0/33.3	11.8/40.1
K2	11.97	2.2/358.4	2.5/9.4	2.6/17.4	2.9/23.9	3.1/29.7

Table 3

Tide height residuals

Pressure gauge	S1	S2	S3	S4	S5	S6	Mean
Residual RMS, cm	8.0	6.6	8.6	7.0	6.6	10.7	7.9
Norm. residual	0.111	0.099	0.136	0.113	0.107	0.172	0.123
Pressure gauge		N2	N3	N4	N5	N6	Mean
Residual RMS, cm		4.5	5.4	5.7	6.5	5.8	5.6
Norm. residual		0.301	0.334	0.317	0.326	0.264	0.308

along the northern line than along the southern line, ranging from 4.5 cm at N2 to 6.5 cm at N5 and 6.2 cm at S2 to 10.7 cm at S6 with means of 5.6 cm and 7.9 cm, respectively. The mean normalized residual for the southern line is 0.123, and thus the predicted tide accounts for about 88% of the overall RMS variability of the sea-surface heights. On the other hand, the predicted tide accounts for only about 70% of the height variability along the northern line due to the primarily much smaller tidal range along the northern section.

4. Tidal currents

Similar to the tidal analyses of the pressure data, tidal analyses of the current data were performed (Foreman, 1978) for the same eight tidal constituents. Major and minor semi-axes, inclination angle (semi-major axis rotation measured in degrees counterclockwise from east), and Greenwich phases for the analyzed tidal constituents computed from vertically averaged currents are given in Table 4. Sense of rotation is indicated by the sign of the minor axis: positive signifies counterclockwise rotation and negative signifies clockwise rotation. Current ellipses are shown for the M2, S2, K1 and O1 components in Fig. 3a–d. Ellipse orientations are along strait except for the Korea end of the southern line for the M2 and S2 ellipses. M2 and S2 ellipses are oriented east–west on the Korea side while they are almost circular on the Japan side of the southern line. Ellipse eccentricity increases across strait towards Japan along the northern line. Ellipse eccentricity generally tends to decrease towards Japan along the southern line. The magnitudes of the M2 velocity ellipses are largest, and are about twice as large as the S2 ellipses. Although the M2 tidal heights are smaller along the north line than on the south line, the M2 ellipses are larger along the north line. Note that the sense of rotation for each of the ellipses is anticyclonic except at S1.

Tidal ellipse parameters are calculated at each depth level. Current amplitudes corresponding to the ellipse major axes and ellipse local inclination angles for the four main constituents (M2, S2, K1, and O1) as a function of depth are shown in Fig. 4. For an entirely barotropic tide the constituent amplitude and inclination angle would appear as vertical lines in Fig. 4.

The M2 current velocity is dominant along the northern section while either M2 or K1 is largest along the southern section. K1 tidal velocities peak between 25 and 40 m along the southern section and are dominant in the surface layer towards the eastern end. M2 velocities along the northern section are larger than along the southern section. The S2 current velocity is the smallest of the four components along the southern line while either S2 or O1 velocities are smallest along the northern section. Differing degrees of bottom and surface boundary effects are evident in each of the constituents. At mid depths, varying degrees of depth dependence are evident.

Inclination angles shown in Fig. 4 have been offset for plotting purposes. The angle ranges are relevant while the absolute magnitudes are not. Vertical inclination angle gradients are largest near the surface and near the bottom. These large gradients imply decreasing velocities and turning of the tidal ellipses. At mid-depths, the ellipse turning is minimal, generally less than 10°. Turning is most pronounced near the bottom. Veering with depth of the diurnal tide is opposite that of the semi-diurnal tide.

Table 4
(a) Tidal current ellipse — ADCP S1

Tide	Period (h)	Major axis	Minor axis	Inc. angle	Greenwich phase
O1	25.82	10.0	1.8	30.4	143.7
P1	24.07	3.1	1.1	26.3	175.1
K1	23.93	11.7	1.7	28.5	172.8
MU2	12.87	0.8	−0.0	9.8	103.9
N2	12.66	3.8	0.6	178.3	315.9
M2	12.42	18.8	3.4	1.7	153.1
S2	12.00	7.4	1.6	175.2	355.8
K2	11.97	1.5	0.2	154.2	349.6

Tidal current ellipse — ADCP S2

O1	25.82	9.9	−0.7	30.3	146.1
P1	24.07	2.9	0.4	29.0	178.5
K1	23.93	11.4	−0.9	31.1	176.2
MU2	12.87	0.7	−0.1	2.1	103.8
N2	12.66	3.4	−0.4	4.2	140.5
M2	12.42	15.3	−1.4	2.5	153.4
S2	12.00	5.8	−0.2	178.9	356.5
K2	11.97	1.2	−0.1	157.9	350.3

Tidal current ellipse — ADCP S3

O1	25.82	9.5	−1.2	34.0	141.5
P1	24.07	2.7	0.3	30.6	174.7
K1	23.93	11.0	−1.4	32.7	172.4
MU2	12.87	0.7	−0.1	178.4	282.4
N2	12.66	2.7	−0.8	1.0	132.2
M2	12.42	12.4	−4.4	179.7	325.2
S2	12.00	4.6	−1.4	174.5	354.8
K2	11.97	0.9	−0.3	153.5	348.6

Tidal current ellipse — ADCP S4

O1	25.82	10.3	−2.4	31.7	138.4
P1	24.07	2.9	−0.0	29.5	169.8
K1	23.93	12.1	−2.8	31.6	167.4
MU2	12.87	0.6	−0.1	10.3	90.4
N2	12.66	2.6	−1.5	2.4	124.7
M2	12.42	11.7	−7.4	0.1	136.8
S2	12.00	4.3	−2.6	175.3	340.8
K2	11.97	0.9	−0.6	154.3	334.6

Tidal current ellipse — ADCP S5

O1	25.82	9.4	−1.3	46.8	163.0
P1	24.07	2.6	0.2	43.1	168.1
K1	23.93	10.6	−1.5	45.2	165.8

Table 4 (Continued)

Tide	Period (h)	Major axis	Minor axis	Inc. angle	Greenwich phase
MU2	12.87	0.6	-0.2	37.5	126.9
N2	12.66	1.9	-1.3	44.0	129.0
M2	12.42	9.5	-6.5	45.3	127.5
S2	12.00	3.5	-2.5	39.5	129.2
K2	11.97	0.7	-0.5	18.5	123.0

Tidal current ellipse — ADCP S6

O1	25.82	11.4	-1.7	40.6	125.8
P1	24.07	3.2	0.3	38.2	158.4
K1	23.93	13.0	-1.9	40.3	156.0
MU2	12.87	0.8	-0.1	18.9	70.2
N2	12.66	2.9	-1.1	26.5	86.3
M2	12.42	12.1	-6.3	32.8	93.1
S2	12.00	4.7	-2.3	28.9	117.6
K2	11.97	1.0	-0.5	7.9	111.4

(b) Tidal current ellipse — ADCP N2

O1	25.82	8.0	-3.5	37.4	118.9
P1	24.07	2.6	-0.6	40.9	151.0
K1	23.93	11.4	-4.9	43.0	148.7
MU2	12.87	1.2	-0.2	49.2	95.1
N2	12.66	4.7	-1.0	51.6	84.1
M2	12.42	23.6	-4.6	56.7	93.6
S2	12.00	10.6	-1.8	56.1	118.9
K2	11.97	2.2	-0.5	35.1	112.7

Tidal current ellipse — ADCP N3

O1	25.82	9.3	-3.1	37.1	155.4
P1	24.07	2.8	-0.6	42.5	160.3
K1	23.93	12.2	-5.0	44.6	157.9
MU2	12.87	1.0	0.0	60.8	149.7
N2	12.66	4.0	-0.6	59.4	141.8
M2	12.42	20.3	-3.2	58.5	136.5
S2	12.00	8.6	-1.2	58.9	135.4
K2	11.97	1.8	-0.3	37.9	129.2

Tidal current ellipse — ADCP N4

O1	25.82	10.0	-3.8	30.2	142.3
P1	24.07	2.8	-0.7	37.5	171.1
K1	23.93	12.4	-5.4	39.6	168.8
MU2	12.87	0.8	0.1	42.1	100.7
N2	12.66	3.7	-0.5	54.3	97.2
M2	12.42	18.5	-3.0	53.1	107.9
S2	12.00	7.9	-1.2	53.3	132.2
K2	11.97	1.6	-0.3	32.3	126.0

Table 4 (Continued)

Tide	Period (h)	Major axis	Minor axis	Inc. angle	Greenwich phase
Tidal current ellipse — ADCP N5					
O1	25.82	10.2	−2.4	38.9	154.2
P1	24.07	2.8	−0.1	41.0	186.8
K1	23.93	11.7	−3.1	43.1	184.5
MU2	12.87	0.7	0.1	51.5	97.8
N2	12.66	3.7	−0.4	54.8	104.1
M2	12.42	17.2	−1.8	56.2	111.7
S2	12.00	7.2	−0.5	54.8	135.7
K2	11.97	1.5	−0.2	33.8	129.5
Tidal current ellipse — ADCP N6					
O1	25.82	11.1	−1.1	44.8	159.8
P1	24.07	3.1	0.2	45.6	195.6
K1	23.93	12.5	−1.9	47.7	193.3
MU2	12.87	0.8	−0.0	54.3	103.4
N2	12.66	3.9	−0.2	55.4	103.4
M2	12.42	18.6	−0.9	54.4	113.4
S2	12.00	7.7	−0.3	54.1	136.4
K2	11.97	1.6	−0.2	33.1	130.2

The predicted tidal currents, u_p and v_p are formed from the eight analyzed tidal constituents. The relative contribution of the tidal currents to the mean kinetic energy can be estimated by the ratio

$$R_{tmke}(z) = \frac{\overline{u_p^2(z)} + \overline{v_p^2(z)}}{\overline{u_o^2(z)} + \overline{v_o^2(z)}}, \quad (2)$$

where u_o and v_o are observed current velocities and the overbar denotes a time mean.

Profiles of R_{tmke} for the north and south lines are shown in Fig. 5 and their mean values are provided in Table 5. The contribution of the tidal currents to the total mean kinetic energy is smallest in the surface layer where the effects of the Korea-Tsushima Current, wind events, and river runoff are strongest. Mean kinetic energy due to tides generally increase with depth outside of strong bottom boundary layers such as suggested at N2. Overall, the contribution of the tidal currents to the total mean kinetic energy is larger along the north line (mean value of 0.49) than along the south line (mean value of 0.37).

Similarly, the contribution of the tidal currents to the mean eddy kinetic energy can be estimated by the ratio

$$R_{teke}(z) = \frac{\overline{u_p'^2(z)} + \overline{v_p'^2(z)}}{\overline{u'^2(z)} + \overline{v'^2(z)}}, \quad (3)$$

where the primed quantities denote deviations from the time mean. The contribution of the tidal currents to the eddy kinetic energy is smallest near the surface. Profiles of R_{teke} have similar shapes along the northern line, have a fairly narrow range (about 0.12) at mid-depth, and are larger

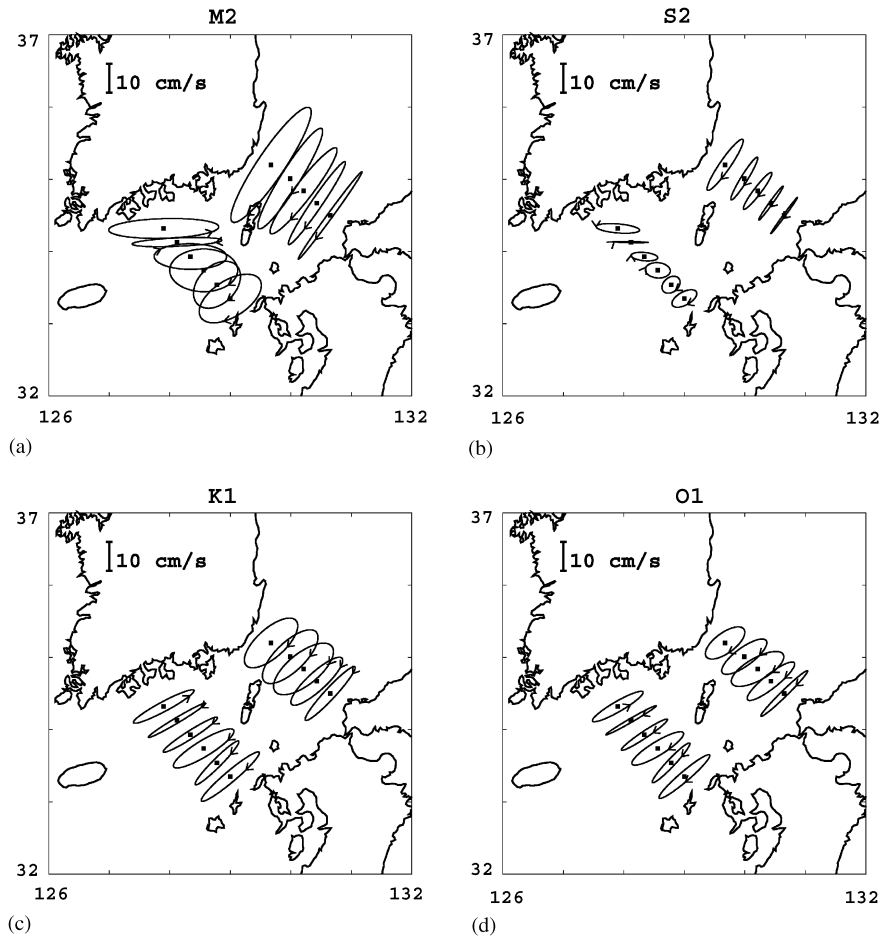
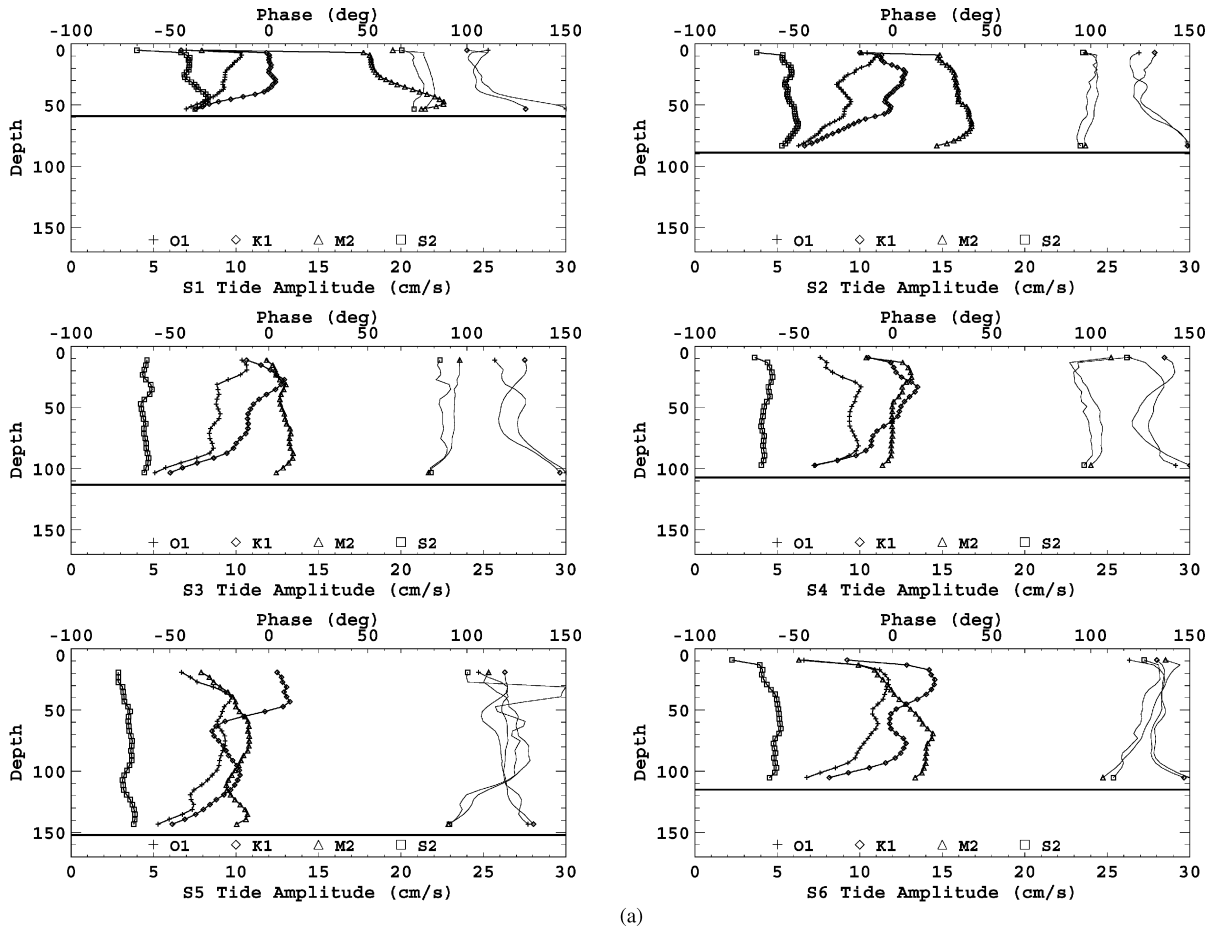


Fig. 3. (a) M2 current ellipses with sense of rotation arrows. (b) As in a but for S2. (c) As in a but for K1. (d) As in a but for O1. The velocity scales are shown in the upper left corner of each panel.

towards Japan. Larger variability is found between profiles of R_{teke} along the southern line. Overall mean values of R_{teke} are smaller along the southern line than along the northern line (0.55 and 0.62, respectively). Note that these measurements were made during May through September. Since each site is stratified in summer and well mixed during winter, R_{tmke} and R_{teke} may vary over an annual cycle. Kang et al. (1995) hypothesized that the interaction between the predominant tidal currents and oceanic currents varying with the seasons might cause a temporal variability in the M2 tide.

5. Discussion

There have been very few long-term measurements of tidal heights and tidal currents in the Tsushima Strait outside of coastal measurements (Odamaki, 1989). Much of the historical tidal



(a)

Fig. 4. (a) Amplitudes of the individual tidal constituents (M2, S2, K1, and O1) corresponding to the magnitudes of the major axes of the tidal ellipses for the southern line. Each computed tidal velocity is marked by an identifying symbol. Corresponding local inclination angles are given by the thin lines marked by symbols at the ends. (b) As in (a) but for the northern line. The bold horizontal line indicates bottom depth.

current observations have been observed by Ekman–Mertz current meters at anchored ship stations which had a duration of only about a day and were sampled at about one hour intervals (Japan Oceanographic Data Center, 1985). From such observations, amplitudes of diurnal and semidiurnal tides can be roughly estimated, but they do not permit estimates of true tidal constituents. In the Strait, Tsushima Current fluctuations make the task of extracting tidal currents from such data more difficult. Magnitudes of the various semidiurnal and diurnal constituents in the middle of the Strait have been inferred from their estimated interrelationships, presumably formed from coastal tide stations. These short-term current observations are also very limited in vertical resolution. Our long-term mooring observations show that the various tidal constituents are not highly barotropic, particularly in the near surface layers where the bulk of the

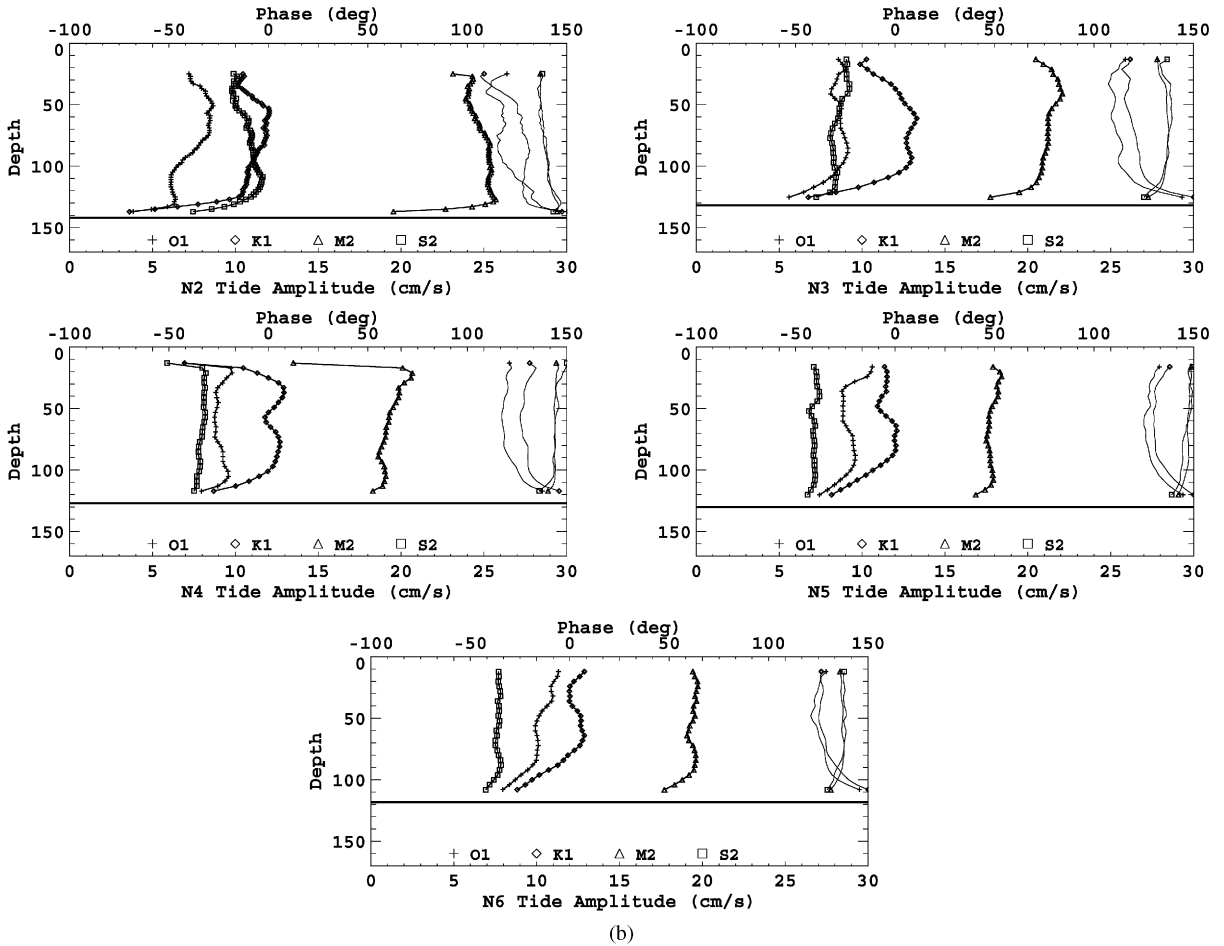


Fig. 4. (Continued)

short-term historical observations are made, and in the near bottom layers. Tidal current and ellipse statistics can be quite different throughout the water column.

Odamaki (1989) analyzed the tides and tidal currents in the Strait using all the data on file at the Japan Oceanographic Data Center and updated the cotidal charts that have been used for more than half a century (Ogura, 1933). Our measurements within the Strait show that some further adjustments to the charts are still needed. Tide amplitudes and phases for the M2, S2, K1 and O1 constituents at the mooring locations from the improved tide charts by Odamaki (1989) are compared with the amplitudes and phases calculated from the pressure data at the moorings in Fig. 6. Amplitudes and phases from the pressure measurements and the chart values show similar trends. Chart amplitudes along the southern line are about 10% high for M2 and S2, and about 10% low for K1 and O1. A maximum difference of 12 cm is observed for the M2 constituent. Along the northern line, absolute differences in amplitudes are generally smaller than on the southern line but reflect a larger percentage of the total amplitude. Phase differences ranged from

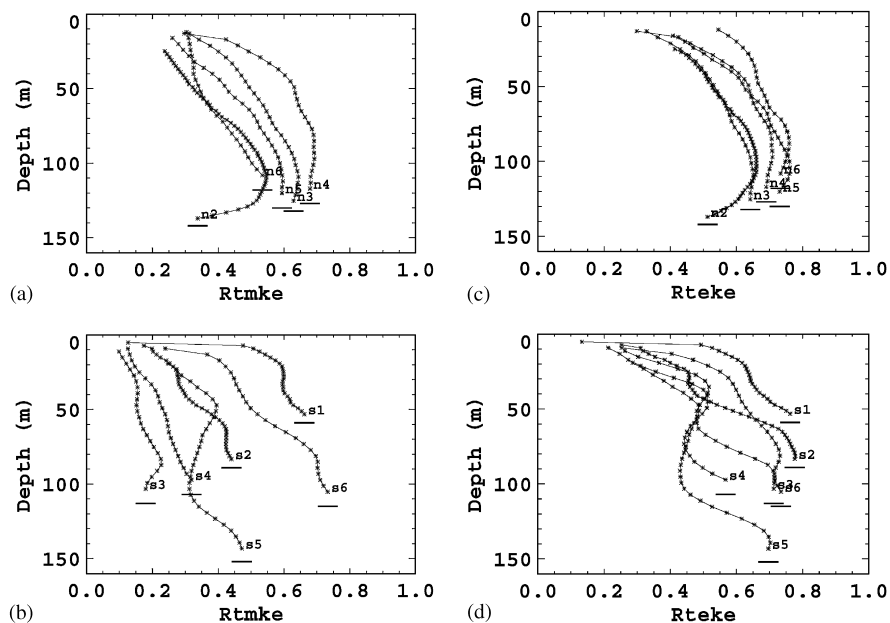


Fig. 5. (a) Contribution of tidal currents to the total mean kinetic energy for the northern line (R_{tmke}). Horizontal bars under each curve indicate bottom depths. (b) As in (a) but for the southern line. (c) Contribution of tidal currents to the total eddy kinetic energy for the northern line (R_{teke}). (d) As in (c) but for the southern line.

Table 5
Tide energy contributions

Pressure gauge	R_{tmke}	R_{teke}
S1	0.57	0.62
S2	0.33	0.56
S3	0.17	0.53
S4	0.23	0.44
S5	0.36	0.49
S6	0.56	0.63
S1–S6	0.37	0.55
N2	0.42	0.58
N3	0.54	0.56
N4	0.62	0.63
N5	0.47	0.65
N6	0.39	0.69
N2–N6	0.49	0.62

a few degrees to as much as 30° at N2 for the K1 constituent. However, the large phase difference is not significant since the amphidromic point for K1 is very close to N2, and is likely closer to N2 than the location shown on the tide charts. These differences in amplitudes and phases are larger than can be accounted for in a seasonal variability of the tides suggested by Kang et al. (1995).

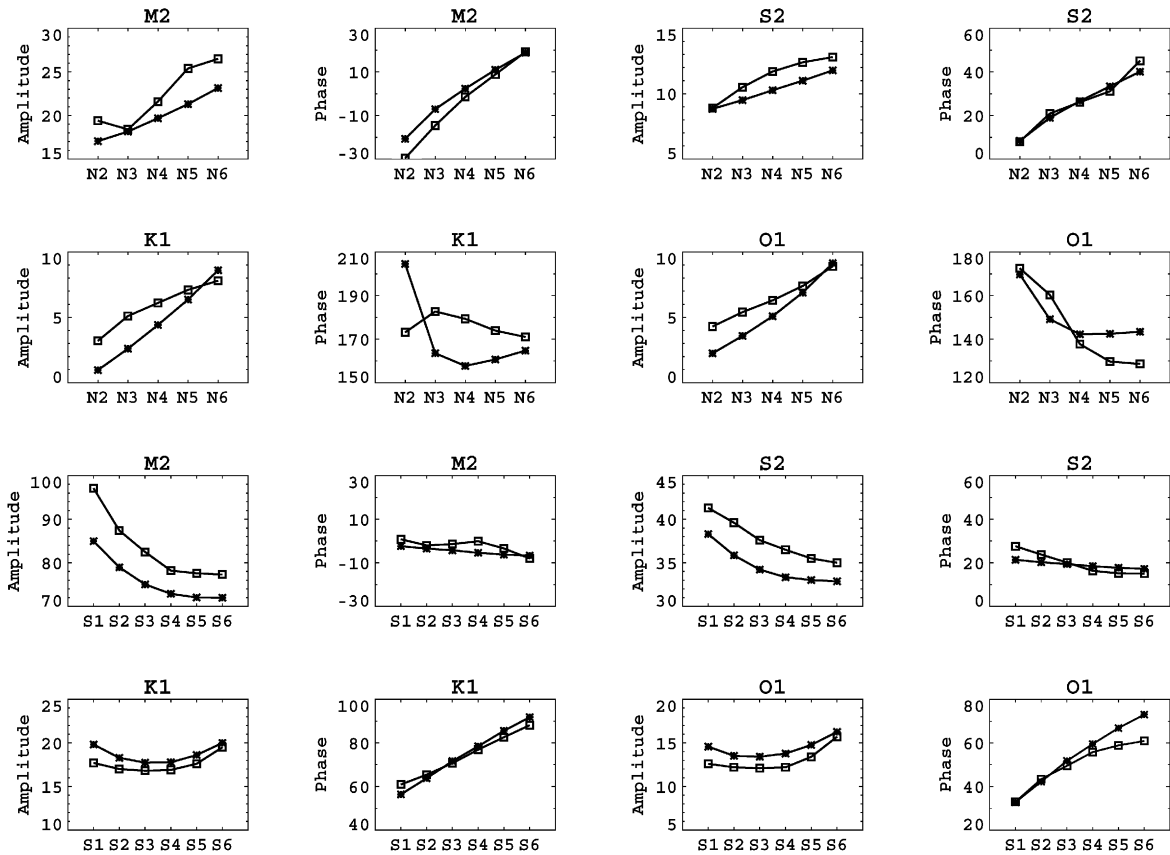


Fig. 6. Tide chart tidal amplitudes (cm) and Greenwich phases (squares) from Odamaki et al. (1989) are compared with computed amplitudes and phases (asterisks) from pressure gauge moorings deployed along lines northeast (N2–N6) and southwest (S1–S6) of Tsushima Island.

One of *Odamaki's* tide stations is located within about 20 km of our S4. Our tidal current amplitudes computed from the long term mooring data are significantly different from his tidal current amplitudes computed from relatively short-term data. For example, his analysis finds M2 amplitudes that are 40% larger than our M2 amplitudes at S4. His next largest constituent is O1, followed by K1, and then S2. We find the largest amplitudes are M2, K1, O1, and S2. His O1 amplitude is approximately twice as large as our O1 amplitude.

The individual tidal constituent amplitudes exhibit varying degrees of depth dependence (Fig. 4). For these ADCP measurements, the velocity level nearest to the surface was located from 5 to 25 m in depth and the velocity level nearest the bottom was located from 5 to 10 m off the bottom. Non-barotropic processes are expected to be more prevalent nearer the surface. As shown here, depth dependence is largest in the surface and bottom boundary layers which are estimated to be between 10 and 30 m in thickness. The M2 constituent, dominant along the northern line, is highly barotropic if the near-surface and near-bottom layers are excluded. The other constituent amplitudes, with the exception of S2, change significantly over depth. Tidal ellipses shown in

Fig. 3 are for the vertically averaged currents and are most representative for the mid-depth tidal velocities. Ellipses for the near-bottom and near-surface regions can be considerably different from those.

Although the tidal height range is much smaller on the northern line than on the southern line, the tidal current velocities are larger along the northern line. The largest tidal current amplitude results from the M2 constituent at N2 on the northern line. Here, the M2 driven velocities exceed 25 cm/s at mid-depth and are about 25% larger than at other locations along the northern line and nearly 50% larger than tidal constituent amplitudes along the southern line.

The contribution of tidal currents to the total velocity field generally increases with depth, with some exceptions in the bottom boundary layer. Tides contribute more to the total velocity field along the northern section than along the southern section (mean R_{tmke} of 0.49 and 0.37, respectively). Tides contribute the least towards the total current at S3 and S4 (Fig. 5) which usually coincide with the core of the Tsushima Current. Tides contribute the most towards the total current at the ends of the southern section (S1 and S6). Along the northern section, tidal currents are most dominant at N3 and N4, located in the regime of highly variable flow with a weak mean flow. Tidal effects are noticeably smaller in the near bottom layer at N2, where significant southward influx of bottom cold water has been observed (Isobe, 1995; Cho and Kim, 1998).

6. Summary and conclusions

Long-term pressure and full-profile current measurements are used within the interior of the Strait to resolve the complex nature of the tides and tidal currents which are embedded in the strong Tsushima Current. Eight tidal constituents account for about 88% of the height variability southwest of Tsushima Island and about 70% of the height variability northeast of Tsushima Island. Chart values of the main tidal constituent amplitudes in the interior of the Strait are high and need some adjustment. M2 and S2 are the dominant height constituents. The M2 constituent dominates the tidal currents northeast of Tsushima Island while either the M2 or K1 dominate the tidal currents southwest of Tsushima Island. Tidal currents account for about 49 and 37% of the total mean kinetic energy and 62 and 55% of the total mean eddy kinetic energy along the north and south lines, respectively. The contribution of tidal currents to the total velocity field generally increases with depth. The main tidal constituents exhibit varying degrees of depth dependence. The M2 constituent is most barotropic along the northern line. Largest depth dependence is found in the near surface and near bottom layers. Vertically averaged tidal velocities may not be representative of the tidal flows, particularly in the surface and bottom boundary layers.

Acknowledgements

This work was sponsored by the Office of Naval Research (program element PE0601153N) as part of the basic research projects “Yellow and East China Seas Response to Winds and Currents” and “Linkages of Asian Marginal Seas”. This work is a contribution of the Naval Research Laboratory (NRL-SSC contribution JA/7332-00-0016).

References

- Cho, Y.-K., Kim, K., 1998. Structure of the Korea Strait Bottom Cold Water and its seasonal variation in 1991. *Continental Shelf Research* 18, 791–804.
- Egawa, T., Nagata, Y., Sato, S., 1993. Seasonal variation of the current in the Tsushima Strait deduced from ADCP data of ship-of-opportunity. *Journal of Oceanography* 49, 39–50.
- Foreman, M.G.G., 1978. Manual for tidal currents analysis and prediction. Pacific Marine Science Report 78-6, Institute of Ocean Sciences, Patricia Bay, Sidney, BC, 70 pp.
- Foreman, M.G.G., Henry, R.F., 1979. Tidal analysis based on high and low water observations. Pacific Marine Science Report 79-15, Institute of Ocean Sciences, Patricia Bay, Sidney, BC, 39 pp.
- Godin, G., 1972. *The Analysis of Tides*. University of Toronto Press, Toronto, Ont., Canada, 264 pp.
- Isobe, A., 1995. The influence of the Bottom Cold Water on the seasonal variability of the Tsushima Warm Current. *Continental Shelf Research* 15, 763–777.
- Isobe, A., Tawara, S., Kaneko, A., Kawano, M., 1994. Seasonal variability in the Tsushima Warm Current, Tsushima-Korea Strait. *Continental Shelf Research* 14, 23–35.
- Jacobs, G.A., Perkins, H.T., Teague, W.J., Hogan, P.J., 2000. Summer transport through the Korea-Tsushima Strait. *Journal of Geophysical Research*, in press.
- Japan Oceanographic Data Center, 1985. Tidal harmonic constants catalogue. JODC Catalogue No. 16, 236 pp.
- Kang, S.K., Chung, J.-Y., Lee, S.-R., Yum, K.-D., 1995. Seasonal variability of the M2 tide in the seas adjacent to Korea. *Continental Shelf Research* 15 (9), 1087–1113.
- Kang, S.K., Lee, S.-R., Yum, K.-D., 1991. Tidal computation of the East China Sea, the Yellow Sea, and the East Sea. In: Takano, A. (Ed.), *Oceanography of Asian and Marginal Seas*. Elsevier, New York, pp. 25–48.
- Katoh, O., Teshima, K., Kubota, K., Tsukiyama, K., 1996. Downstream transition of the Tsushima Current west of Kyushu in summer. *Journal of Oceanography* 52, 93–108.
- Kawatate, K., Miita, T., Ouchi, Y., Mizuno, S., 1988. A report on failures of current meter moorings set east of Tsushima Island from 1983 to 1987. *Progress in Oceanography* 21, 319–327.
- Mizuno, S., Kawatate, K., Nagahama, T., Miita, T., 1989. Measurements of East Tsushima Current in winter and estimation of its seasonal variability. *Journal of the Oceanographic Society of Japan* 45, 375–384.
- Odamaki, M., 1989. Tides and tidal currents in the Tsushima Strait. *Journal of the Oceanographic Society of Japan* 45, 65–82.
- Ogura, S., 1933. The tides in the Seas adjacent to Japan. *Japanese Bulletin Hydrographic Department* 7, 1–189.
- Perkins, H., de Strobel, F., Gualdesi, L., 2000a. The Barny Sentinel Trawl-resistant ADCP bottom mount: design, testing, and application. *IEEE Journal Oceanic Engineering*, accepted for publication.
- Perkins, H.T., Teague, W.J., Jacobs, G.A., Chang, K.I., Suk, M.-S., 2000b. Currents in Korea-Tsushima Strait during summer 1999. *Geophysical Research Letters* 27, 3033–3036.
- Teague, W.J., Jacobs, G.A., 2000. Current observations on the development of the Yellow Sea Warm Current. *Journal of Geophysical Research* 105 (C2), 3401–3411.
- Teague, W.J., Perkins, H.T., Hallock, Z.R., Jacobs, G.A., 1998. Current and tide observations in the southern Yellow Sea. *Journal Geophysical Research* 103, 27,783–27,793.